JOURNAL OF GEOPHYSICAL RESEARCH, VOL. 104, NO. C11, PAGES 25,747–25,759, NOVEMBER 15, 1999

Area balance of the Arctic Ocean perennial ice zone: October 1996 to April 1997

R. Kwok, G. F. Cunningham, and S. Yueh

Jet Propulsion Laboratory, California Institute of Technology, Pasadena

Abstract. We use National Aeronautics and Space Administration scatterometer (NSCAT), RADARSAT, and ice motion data to examine the perennial ice zone (PIZ) of the Arctic Ocean between October 1996 and April 1997. The PIZ is identified by a simple backscatter-based classification of the gridded NSCAT backscatter fields. The area of the PIZ at the beginning of October occupies an area of 5.32×10^6 km^2, ~76% of the Arctic Ocean. By the first of May, only 4.54×10^6 km^2 of that area remains, a decrease of 0.78×10^6 km^2 over the 7-month period. This area loss can be explained almost entirely by ice export. Over this period the total area flux of sea ice through Fram Strait, estimated using satellite passive microwave ice motion, is 0.80×10^6 km^2 or 12% of the Arctic Ocean. Approximately 0.70×10^6 km^2 or 88% of the exported area is from the PIZ. Nares Strait outflow is small at 34,000 km^2 and is estimated by summing the high backscatter areas exported into northern Baffin Bay. After accounting for the outflow through the Fram and Nares Straits an unexplained residual of 46,000 km^2 remains. We attribute this residual to errors in our estimation process, the unaccounted for ice flux through the Canadian Archipelago, and the net divergence and convergence of the PIZ over the period. Our interpretation of the radiometry seems to be sound on the basis of the area balance arguments provided here. This study shows that (1) the PIZ converage of the Arctic Ocean can be derived from NSCAT backscatter fields and (2) the decrease in PIZ area over the winter is a good estimate of the PIZ net ice area exported through Fram Strait.

1. Introduction

An important property that distinguishes multiyear ice from first-year ice is thickness. Multiyear ice is thicker because its greater age corresponds to a larger cumulative energy deficit at the surface and therefore more growth by freezing. The climatic significance of multiyear ice coverage of the Arctic Ocean can be attributed to its strong relation to the summer ice concentration [*Comiso*, 1990; *Thomas and Rothrock*, 1993]. If changes in the climate cause persistent decreases in the summer ice concentration, it would be reflected in decreases in the winter multiyear ice coverage. This reduction would be due to increased melt during the previous summer or ice export through the Fram Strait. The outflow of primarily thick multiyear ice into Fram Strait represents a major source of surface fresh water for the Greenland-Iceland-Norwegian Seas, which are source regions of much of the deep water in the world's oceans [*Aagaard and Carmack*, 1989].

An accurate record of the multiyear ice coverage and its variability is therefore important to understanding the relationship between climate and multiyear ice balance. An adequate description of the sea ice cover requires the relative proportions of first-year (FY) and multiyear (MY) ice to be known as a function of time. Even though the distinction between the two ice types is relatively simple, estimates of the relative coverage of the two ice types in the Arctic Ocean have been difficult to obtain. Ice-type retrieval algorithms (e.g., the Team algorithm) using satellite microwave data [*Cavalieri et al*., 1984] have been shown to be unreliable [*Carsey*, 1982; *Comiso*, 1986; *Thomas*, 1993] because of the following shortcomings: (1) the retrieved MY ice fractions in the winter are much lower than those retrieved in the summer and significantly lower than independent estimates [*Wittmann and Schule*, 1966; *Beaven et al*., 1996], and (2) the variability in ice-type fractions appears to be caused by spatial and temporal variations in the assumed signatures. In a year-long comparison of ice-type retrieval results obtained from synthetic aperture radar (SAR) and satellite passive microwave data, *Kwok et al*. [1996] show that the results of SAR retrieval produce higher and temporally less variable MY fractions over the winter. This study was, however, limited to the Beaufort Sea because of the unavailability of SAR data in other regions of the Arctic Ocean. *Thomas and Rothrock* [1993] used a Kalman filter/smoother to couple a physical model and the Team algorithm analyses to obtain optimal estimates of the total ice and MY ice fractions to overcome the inconsistencies in the temporal record. The filtering procedure increases the winter MY ice fraction and decreases the summer ice fraction to reduce the inconsistency between the summer and winter concentration estimates derived from passive microwave data. Although this consistency condition is satisfied, they note that the filtered estimates would be biased if the measurements were themselves biased.

Our contribution to the topic brings to bear three relatively new data sets: National Aeronautics and Space Administration scatterometer (NSCAT) backscatter fields of the Arctic Ocean, ice motion derived from satellite passive microwave imagery, and SAR imagery from RADARSAT. The contrast between the perennial and seasonal ice zones in the NSCAT fields are

Paper number 1999JC900234.
0148-0227/99/1999JC900234$09.00

high and distinctive, thus allowing easy delineation of the two ice zone using a simple thresholding algorithm. We use the RADARSAT data and ice motion fields from passive microwave data to study and validate the temporal behavior of the derived PIZ. We show, through area balance, that the derived area of the PIZ indeed provides a reasonable estimate of the MY fraction of the Arctic Ocean over the 7-month period.

In section 2 the three data sets used in our analysis are described. The K_u band backscatter fields of the Arctic Ocean are new, and they are synthesized directly from NSCAT observations. In section 3 we point out the features of the ice cover that can be observed in these time-sequential fields between October 1996 and April 1997. Even though the spatial resolution of the data is fairly coarse, the coverage of the data and the stability of the backscatter over the 7-month period are valuable for inferring changes in the ice cover. In section 4 the objective procedure for identification of the perennial ice zone (PIZ) in the NSCAT fields is described. In section 5 we analyze the temporal behavior of the PIZ area within the Arctic Ocean by considering the convergence/divergence of the PIZ and the export of PIZ area through different passages out of the Arctic Ocean. The decrease in area of the PIZ over the 7-month period is explained, to within the uncertainty in the estimates, by ice export and ice cover deformation. Our time series of the PIZ area are compared to MY ice coverage derived from passive microwave fields and model estimates from other investigations. In section 6 the paper is summarized.

2. Data Description

2.1. NSCAT Backscatter Fields

NSCAT is a K_u band scatterometer on board the Japanese ADEOS platform. The primary mission of this instrument is to measure wind over the ocean surface. The scatterometer uses six fan beam antennas illuminating two 600-km swaths on each side of the spacecraft ground track [*Naderi et al*., 1991]. The fore and aft antennas operate at vertical polarization, while the midbeam antennas can transmit and receive vertically or horizontally polarized waves. The data have a spatial resolution of 7 km $\times$ 25 km after radar processing. For consistent wind estimates the backscatter measurements are calibrated to better than 0.25 dB.

The fields of normalized backscatter of the Arctic Ocean created here (Plate 1) are sampled on a 12.5 km by 12.5 km Special Sensor Microwave Imager (SSM/I) polar stereographic grid. The near-simultaneous NSCAT measurements from all the antenna beams are combined to estimate the 50° incidence angle backscatter at each grid point. To do this, we assume a linear relation [*Yueh et al*., 1997],

$$\sigma_0(\theta) = A + B(\theta - 50) \text{ dB} \quad (1)$$

between backscatter σ_0 and incidence angle θ (degrees). Available measurements for determining the regression coefficients A and B are weighted by the fractional area of NSCAT resolution cells falling inside the 12.5 km $\times$ 12.5 km grid cells. Each backscatter field is constructed from the accumulation of ~3 days of NSCAT observations of the Arctic Ocean. Results from a simple and effective ice/open ocean classifier [*Yueh et al*., 1997; *Yueh and Kwok*, 1998] are used to mask out areas of open water (colored blue in Plate 1). In this algorithm a pixel is classified as sea ice if A is between -25 and 0 dB and the midbeam polarization ratio (vertical transmit and receive polarization (VV)/horizontal transmit and receive polarization (HH)) is between -3 and 2 dB. Otherwise, it is classified as open water.

An advantage of NSCAT measurements is that they are relatively free from atmospheric contamination. *Liebe* [1985] shows that the attenuation of K_u band waves due to a moist atmosphere is negligible compared to the calibration requirements of the sensor (0.2 dB). As a point of reference, the round-trip attenuation due to a U.S. standard atmosphere at the NSCAT wavelength and incidence angles is ~0.1 dB. The effect due to clouds is also small: *Ulaby et al*. [1981] report that the attenuation coefficient of ice clouds and water clouds varies between 0.001 and 0.1 dB km^{-1} g^{-1} m^3.

2.2. RADARSAT Images

The SAR data used here are calibrated, processed, and archived at the Alaska SAR Facility (ASF) in Fairbanks. The RADARSAT C band imaging radar transmits and receives HH. The imagery used here (resolution ~150 m) is collected by the radar operating in one of its multibeam modes, which illuminates a 460-km wide ground swath. The incidence angle within the swath varies over a range of 20°–44°. The data from the ASF SAR processor have an absolute calibration accuracy of 2 dB and a relative calibration accuracy of 1 dB.

2.3. SSM/I Ice Motion

The 1-day ice motion fields are derived from sequential SSM/I brightness temperature fields. Procedures used to construct these motion fields are described by *Kwok et al*. [1998]. Individual motion vectors are expected to have uncertainties of 5–6 km d^{-1}. Uncertainties in average ice motion over a longer time period are lower since the error statistics are normally distributed.

3. NSCAT Backscatter Fields

NSCAT was operational between September 1996 and June 1997. For this study we constructed 90 backscatter fields of the Arctic Ocean spanning October through April. A subset of the fields that illustrate the time-dependent backscatter behavior of the ice cover are shown in Plate 1. We selected the period between October 1996 and April 1997 for our analyses to avoid temperature-induced transients in sea ice backscatter near the seasonal transitions in September and June. MY ice backscatter tends to remain stable when the near-surface air temperature remains below -10°C. In this section we provide somewhat qualitative observations of the backscatter time series that are treated in more detail in the following sections.

The time series shows a significant backscatter contrast (4–7 dB) between the PIZ and the seasonal ice zone (SIZ) that is persistent throughout the year. The PIZ is mostly covered by MY ice, whereas the primary ice type in the SIZ is FY ice. The scattering from the inhomogeneities in the low-salinity MY ice volume, snow grains, hummocks, and ridges within an NSCAT resolution element give the ice cover a characteristic high backscatter. The FY ice cover has a lower backscatter because this higher-salinity ice type causes surface backscatter to be the dominant component of the radar return. The backscatter level within the two zones remains remarkably stable throughout the season (also see Figure 4). Growth in the area of the SIZ (low-backscatter regions) over the winter is evident over the 7-month sequence. The areal coverage of FY ice in the SIZ is small at the end of summer but increases rapidly after fall

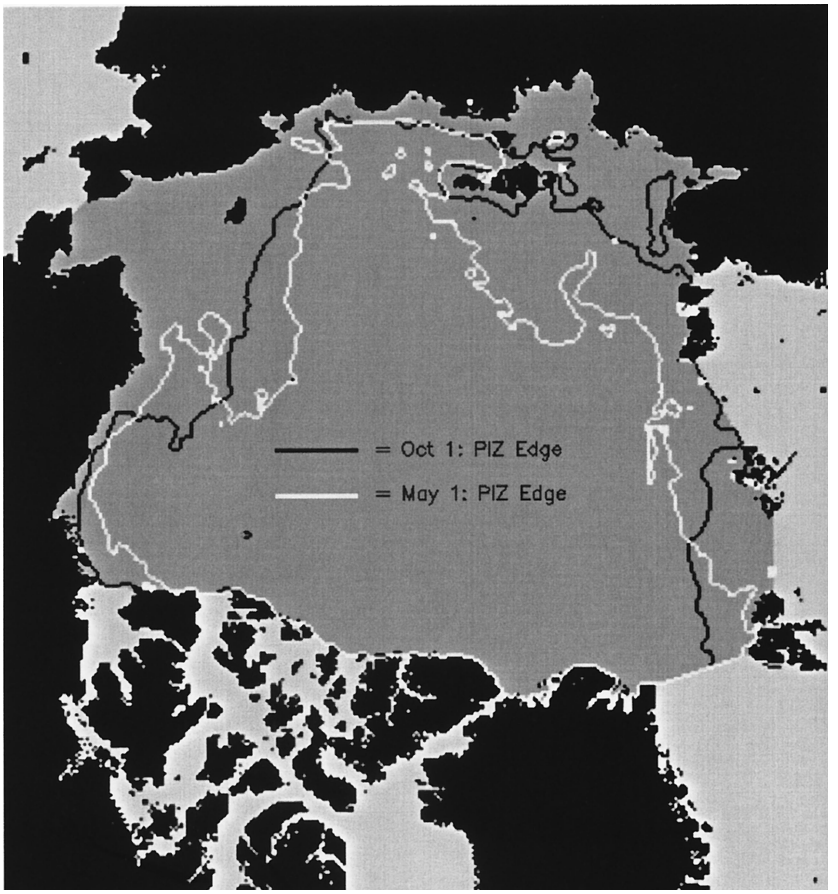

Figure 1. The Arctic Ocean domain. Also shown are the boundaries of the perennial ice zone (PIZ) on October 1, 1996, and May 1, 1997.

freeze-up. Over the winter, there is a slow decrease in the PIZ coverage of the Arctic Ocean. Animation of the time sequence of NSCAT backscatter fields suggests export of high-backscatter PIZ ice through Fram Strait. The East Greenland Current then carries this ice south toward the Denmark Strait. In the East Greenland Sea the areal coverage of the high-backscatter ice from the Arctic Ocean PIZ increases quickly at first but slows after mid-January. The Odden ice tongue in the Greenland Sea, which failed to develop during both 1994 and 1995, is noticeable from mid-November through early April, although it is not clear whether any of the MY ice advects into the ice tongue. There is no visually observable outflow of sea ice from the PIZ through the Bering Strait or the passages into the Barents and Kara Seas. Outflow through the Nares Strait is evident in the animation. High backscatter ice drifting through the strait are periodically "calved" off of the ice area near the southeast coast of Ellesmere Island.

We use this data set to study the evolution of the area of the PIZ from October 1996 through May 1997. To determine whether this data set is useful quantitatively, we pose the following questions: Is it possible to define the boundaries of the PIZ objectively over the study period?; Is the backscatter of the PIZ stable throughout the season?; and Can the change in area of the PIZ over the Arctic Ocean be explained by ice export and convergence/divergence of the ice cover? The answer to the last question allows us to decide whether our analysis provides a quantitative description of the PIZ coverage of the Arctic Ocean.

4. Definition of the Perennial Ice Zone (PIZ)

We analyze the area of the PIZ within the boundaries of the Arctic Ocean domain shown in Figure 1. The area of the PIZ is defined as the sum of the area of all pixels above a certain backscatter threshold. The estimation of this threshold is discussed below.

4.1. Time-Dependent Threshold

The large spatial gradient in backscatter in the transition region between the perennial and seasonal ice zones provides a clear definition of the edge of the PIZ. Figure 2 shows this transition region in an NSCAT backscatter field and a coincident RADARSAT image. The −12 and −13 dB NSCAT backscatter isopleths are overlaid on both images. Although there is a large disparity between the resolution of the two sensors, the general correspondence between spatial and radiometric content of the imagery is good. Figure 3 shows the backscatter values of ice mixtures (MY and FY ice) in the SIZ and PIZ from four RADARSAT/NSCAT image pairs. By definition, MY ice is the principal ice type in the PIZ, whereas FY ice is the principal ice type in the SIZ. The results show that the C band contrast between the two ice zones is ~2–3 dB, while the higher contrast at K_u band ranges from 4 to more than 7 dB. The contrast at C band is slightly lower than that observed by *Kwok and Cunningham* [1994] because of the mixing of deformed and undeformed ice over the large areas sampled here. *Kwok and Cunningham* [1994] studied the backscatter of rela-

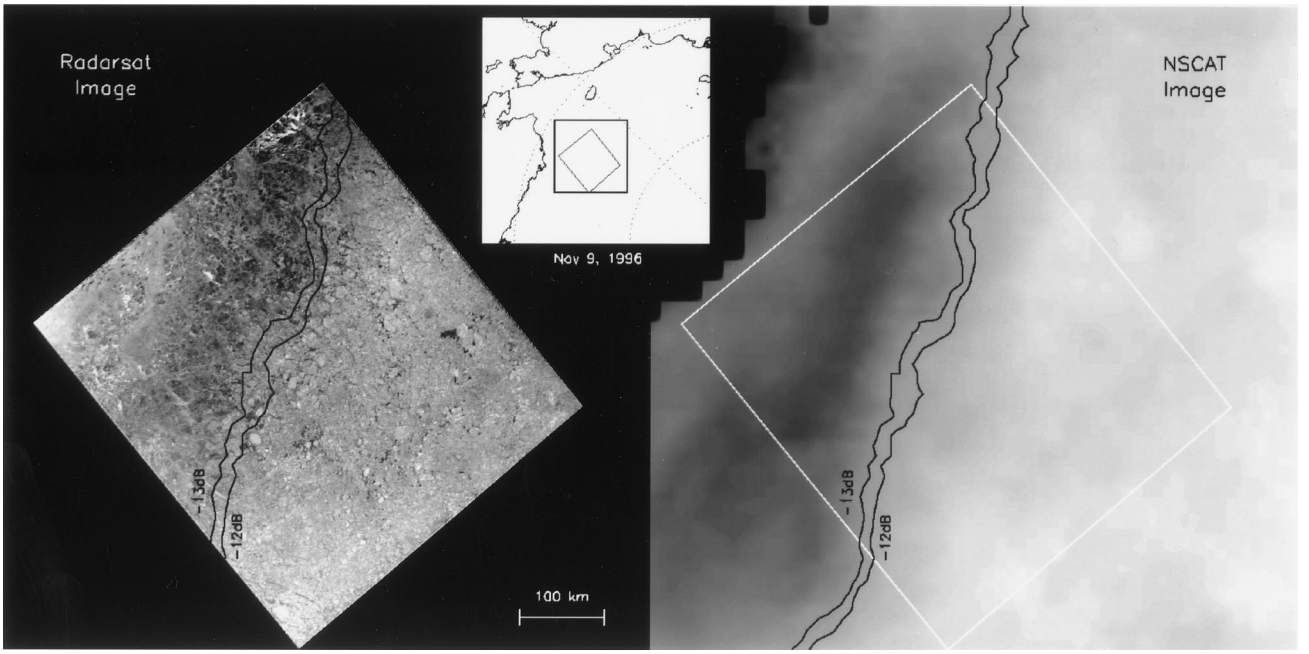

Figure 2. RADARSAT synthetic aperture radar (SAR) imagery and NSCAT backscatter field showing the transition between the PIZ and seasonal ice zone (SIZ) (time and date). Backscatter isopleths (−12 and −13 dB) on the RADARSAT image are derived from the colocated NSCAT backscatter field. (RADARSAT imagery ©CSA 1999)

tively pure MY and FY areas. This higher contrast in the NSCAT data allows us to approximately identify the boundary between the ice zones. Other investigators [*Long and Drinkwater*, 1999; *Remund et al*., 1998] have also exploited this distinctive contrast in the K_u band data to extract information relating to ice type and ice extent.

The enhanced K_u band contrast of PIZ and SIZ ice at 50° incidence over that of the C band can be explained as follows. For low-salinity MY ice we believe enhanced contribution of volume scattering from the inhomogeneities increases backscatter at the shorter K_u band wavelength. The lower K_u band backscatter of FY ice is probably due to a further decrease in the volume scattering contribution to the total radar return due to decreased penetration. Moreover, lower backscatter from FY ice in the higher incidence angle NSCAT measurements is expected. Throughout the season, two well-separated and distinct peaks associated with FY and MY ice can be seen in the backscatter distributions (Figure 4). Further discussions of the behavior of these distributions are provided below.

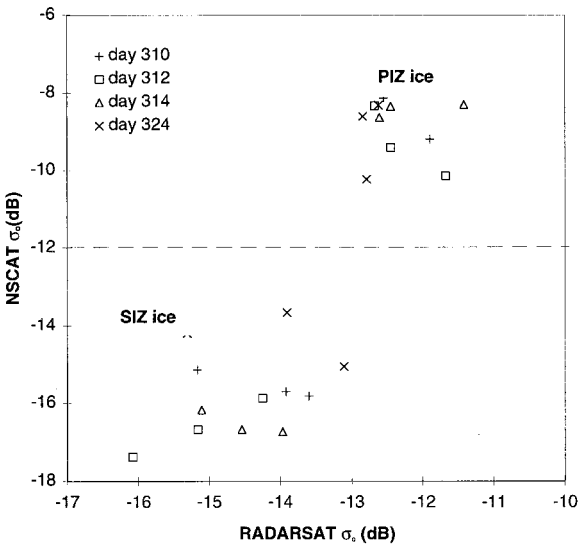

Figure 3. Average backscatter over seasonal and perennial ice areas (sample area ~ 5000 km^2) extracted from four RADARSAT/NSCAT image pairs. The samples from the PIZ and SIZ are separated by the dashed line.

We employ the following procedure to obtain an objective estimate of the backscatter threshold to determine the PIZ area. The average of the backscatter values at the locations of maximum gradient over an NSCAT backscatter field is selected as the threshold for that image. Vector gradients are computed by taking the central differences (separation = 50 km) along two orthogonal axes defined by the image coordinate system. The peaks are well-defined in the cases we examined, and the magnitude of these peaks are typically 5 dB/100 km. A plot of these backscatter thresholds sampled twice a month (Figure 5) shows a time-dependent trend, ranging from ~−12 dB in early October to −13 dB in May. The standard deviation is 0.26 dB. This unexpected trend is also evident in the leftward shift of backscatter population in the distributions shown in Figure 4. In order to eliminate the possibility of a slow drift in the NSCAT sensor calibration we examine the time dependence of the K_u band backscatter of a 30,000-km^2 area in northeast Greenland that is above the 2-km elevation contour. The backscatter from this cold, low accumulation, dry snow zone should remain very stable during the winter. Indeed, over the winter the trend in backscatter is negligible (within the calibration accuracy of 0.25 dB) compared to the more than 1 dB decrease over the sea ice cover within the PIZ (Figure 6). It is important to note here that this decrease in backscatter is not a local effect, as it is observed over the entire PIZ ice cover.

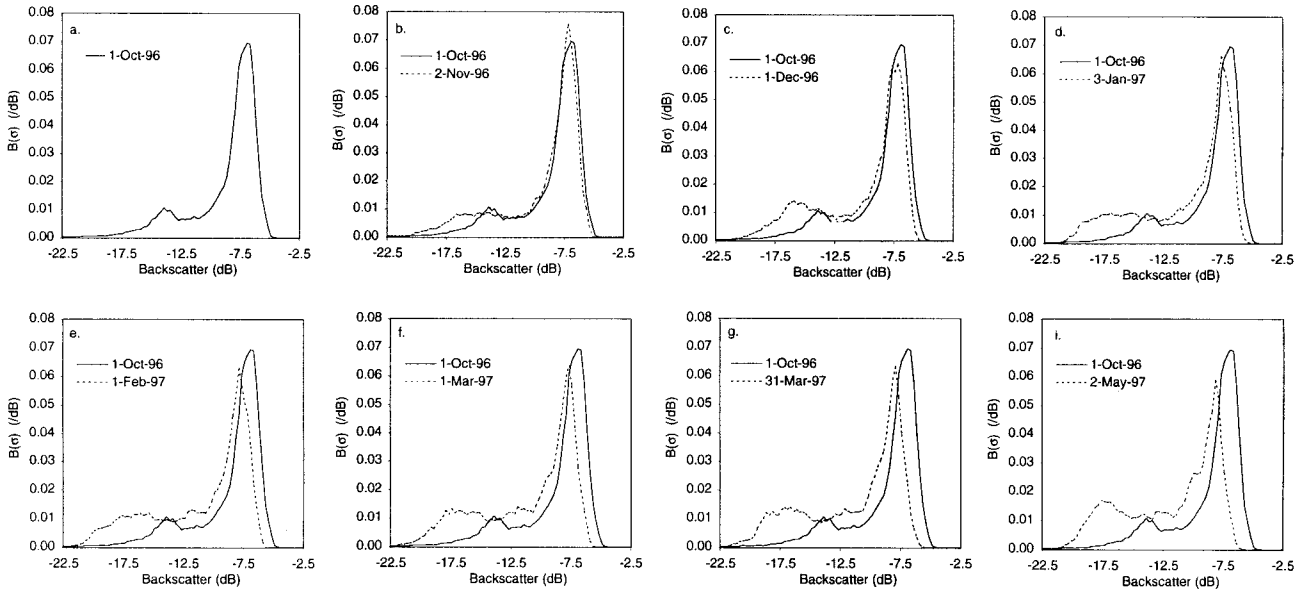

Figure 4. Distributions of backscatter within our domain: (a) October 1, 1996, (b) November 2, 1996, (c) December 1, 1996, (d) January 3, 1997, (e) February 1, 1997, (f) March 1, 1997, (g) March 31, 1997, and (h) May 2, 1997. To show the changes in the distributions over time, the backscatter distribution from October 1, 1996 (solid line), is shown in each plot. Ice export from the PIZ reduces the size of the high-backscatter peak. This area is replaced with FY ice. (Bins are 0.25 dB.)

On the basis of the above discussion we conclude that this trend is probably a natural phenomenon (discussed in more detail below) and not likely to be a measurement artifact. Hence the coefficients from regression of the measured threshold against time are used to determine the linear time-dependent thresholds used in computing the PIZ area. We note that the trend of sea ice backscatter in the SIZ also shows a small decreasing trend (<1 dB) over the 7 months. The backscatter variability of sea ice in the SIZ is, however, higher because of the mix of FY ice with different backscatter characteristics.

Two sources of error affect the uncertainty in the PIZ area: (1) the variability of the thresholds (0.26 dB) and (2) the effect of calibration of the backscatter measurements (0.25 dB) on threshold determination. Together they introduce an uncertainty of ~106,000 km^2 or 1.8% in the determination of the PIZ area.

We use RADARSAT imagery to obtain a more quantitative estimate of the MY fraction one expects to find within the PIZ. The MY ice fraction is determined using a simple classifier outlined by *Kwok et al.* [1992]. From four coincident NSCAT and RADARSAT images we find the MY fraction within 100 km of the PIZ boundary to be between 0.90 and 0.94. We expect the MY fraction in the interior of the PIZ to be higher.

4.2. Decrease in Backscatter Over the 7 Month Period

The decrease in backscatter over such a large area of the ice cover is interesting. Net divergence would introduce ice with lower backscatter into PIZ, thus reducing its average backscatter. However, it is unlikely that net divergence could alone account for this magnitude of backscatter decrease. Assuming a linear mixing of the normalized backscatter power of MY(P_{MY}) and FY(P_{FY}) ice, the total observed power at the radar, P_{tot}, is given by

$$P_{tot} = \alpha P_{MY} + (1 - \alpha) P_{FY}, \quad (2)$$

where α is the MY fraction. The average backscatter of the sea ice within the PIZ and SIZ is ~−8 dB and −15 dB, respectively. These are obtained by averaging the backscatter of the sea ice within the two zones. With a ratio P_{MY}/P_{FY} of 5.0 the total power is not sensitive to small fractions of FY ice. It would take a large fraction of FY ice coverage to affect P_{tot}. For instance, more than a 30% net divergence of the PIZ ice cover is required to reduce the observed backscatter by 1 dB. We also show in the next section that the net divergence/convergence within the PIZ is probably quite small (1–2%).

We speculate that this trend in the backscatter might be related to snow cover, more specifically, to changes at the snow-ice interface. It is unlikely that the snow cover will have a large effect because the attenuation of cold, dry snow at the K_u band is negligible. At the end of the summer the surface of

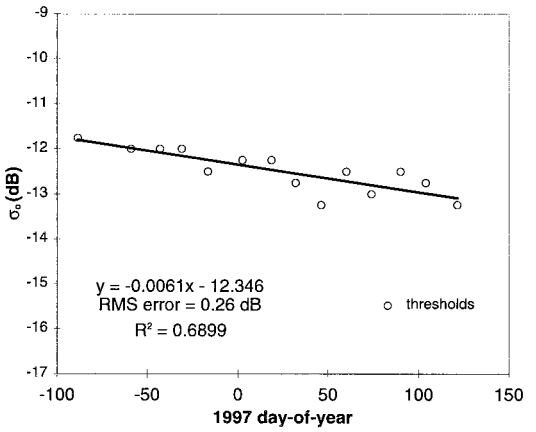

Figure 5. Trend of backscatter thresholds used to determine the area of the PIZ. The day of year is relative to January 1, 1997.

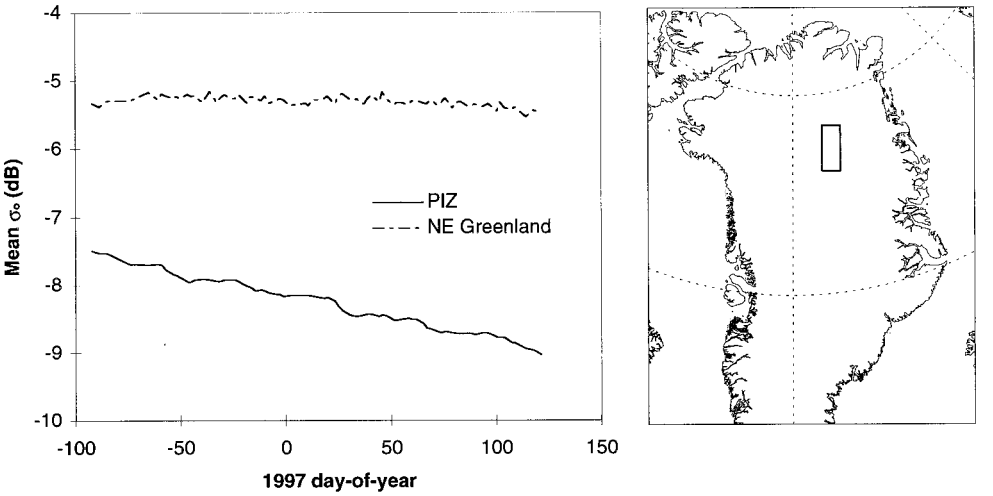

Figure 6. Comparison of the variability of the backscatter of an area of ~30,000 km^2 over (right) northeast Greenland and the backscatter within the PIZ as defined by the time-varying thresholds in Figure 4.

the ice cover is relatively bare. Snow accumulation over the surface and the changes of the snow-ice interface, for example, formation of depth hoar during the winter would have a more definite effect on the scattering properties of the ice cover. For a decrease in backscatter to occur the changes at the snow-ice interface would have to reduce the contribution of scattering from the ice volume, thus reducing the overall backscatter of the older ice. We are not, however, aware of any studies in the published literature detailing the evolution of the physical properties of the snow-ice interface over the winter.

5. Area Balance of the PIZ

The area of the PIZ from October 1996 through April 1997 based on our analysis is shown in Figure 7. At the beginning of October the area of the PIZ is ~5.32 × 10^6 km^2, occupying ~76% of the Arctic Ocean. By the first of May the remaining area is 4.54 × 10^6 km^2, a loss of 0.78 × 10^6 km^2 over the 7-month period. The variability in the PIZ area superimposed on the downward trend is 62,000 km^2, ~1.3% of the average PIZ area. The boundaries of the PIZ at the beginning of October 1996 and May 1997 (Figure 1) show the westward advection of ice as part of the Beaufort Gyre and the northward motion of the PIZ edge in the Eurasian Basin.

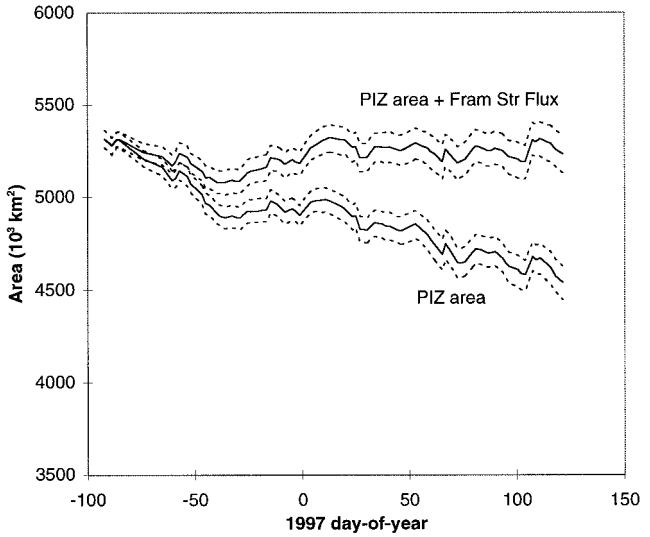

Figure 7. PIZ area and sum of the PIZ area and the area flux through Fram Strait derived from satellite passive microwave ice motion over the 7-month period. The area flux is computed along a line roughly parallel to 81°N from Greenland to northeastern Svalbard. Dashed lines indicate the uncertainty in the determination of the PIZ area due to calibration and uncertainty in threshold estimates.

In this section the area loss from the PIZ is examined. If we consider the area balance of the PIZ within the Arctic Ocean domain to be affected by only export and deformation, then the area of the PIZ at time t can be written as

$$A_{\mathrm{PIZ}}(t) = A_{\mathrm{PIZ}}(0) - [A_{\mathrm{export}}(t) + A_{\mathrm{def}}(t)]. \quad (3)$$

A_{export} is the net export of the PIZ area through the different passages in the Arctic Ocean, and A_{def} is the net area change of the PIZ due to convergence (ridging) and divergence (opening of leads). Net melt of MY ice is assumed to be zero, a reasonable assumption in the winter Arctic Ocean.

5.1. Ice Export

The passages out of our Arctic Ocean domain bordering the PIZ are Fram Strait, Nares Strait, and the openings into the Canadian Archipelago. There is no visually observable outflow of sea ice from the PIZ through the Bering Strait and the passages into the Barents and Kara Seas, so the PIZ ice flux through these passages is not considered here.

5.1.1. Fram Strait. We estimate the area flux of ice through Fram Strait using the procedure described by *Kwok and Rothrock* [1999]. Briefly, daily ice motion over an area of ~780 km × 780 km centered around Fram Strait is derived from sequential SSM/I 85 GHz V records over the 7-month period. The area flux is estimated at a gate positioned along a 400-km line, roughly along 81°N, drawn across the passage between Antarctic Bay off the northeast coast of Greenland and the northwestern tip of Svalbard. Ice export is estimated by integrating the ice motion over 20 sample points along the flux gate using the simple trapezoidal rule.

Ice area export through Fram Strait should be the largest component of the A_{export} term in the area balance. Figure 8

shows the area flux through Fram Strait between October 1996 and April 1997. The total ice area exported over the 7 months is 798,000 km^2. The uncertainty in this ice flux estimates is ~4% of the total area flux [*Kwok and Rothrock*, 1999]. To estimate only the PIZ component of this outflow, we weigh the cross-strait velocity profile by the PIZ pixels crossing the flux gate. Over 88% of the total area flux is from the PIZ. This results in a PIZ export through the Fram Strait of ~697,000 km^2. The average backscatter profile of the sea ice along the flux gate is shown in Figure 9. The high-backscatter ice in the western part of Fram Strait is from the PIZ in the Arctic Ocean and has large MY ice fractions, while the source of the lower backscatter seasonal ice has advected westward from the Arctic Ocean north of the Barents and Kara Seas.

5.1.2. Nares Strait. Animation of the NSCAT backscatter fields reveals outflows of ice through the Nares Strait between the northwest coast of Greenland and Ellesmere Island. Figure 10 shows an NSCAT backscatter field and a coincident RADARSAT image of the opening into Nares Strait (~30-km wide) in the Arctic Ocean. The high-resolution SAR image shows the characteristic "arch" feature, also evident in the NSCAT data, formed from leads at the opening into this narrow passage. Note that the perennial pack does not move through the strait as an unbroken ice cover. Rather, leads form in the perennial pack as floes are broken off the arch and exported through the passage. This causes the Nares Strait outflow into Baffin Bay to have an increased fraction of FY ice. In the lower-resolution NSCAT fields the evidence of outflow is apparent in both the periodic appearances of low-backscatter features (the arch) in the ice cover of the Lincoln Sea and the outflow of PIZ ice from the Nares Strait into northern Baffin Bay (see Plate 1). However, a direct measurement of the ice motion into the Nares Strait cannot be made in the same manner as that of the Fram Strait. This passage is too narrow compared to the resolution of the 85-GHz passive microwave data. Our approach is to measure the outflow at the opening of Nares Strait into Baffin Bay.

The NSCAT fields show relatively large areas of ice, with backscatter values similar to those in the PIZ, clearly flowing through the Nares Strait into upper Baffin Bay. We compute this ice area within a spatial window using the thresholds defined above. The area of the PIZ ice in this region is shown Figure 11. Note that the region within the window excludes any possible outflow of PIZ ice from Lancaster Sound. The results show that there are periodic episodes of higher areal coverage by PIZ ice. Examination of the animation reveals that the maxima in the plots coincide with times when large areas of bright ice appear to have calved from the mouth of the strait and moved southward into Baffin Bay. Summing the areas at these peaks then gives us an estimate of the total ice area transported through Nares Strait. Note that the earliest peak in early October corresponded to high-backscatter sea ice entering the region from the southeast and is ignored. However, the double peaks in early March, though near each other in time, represent unique areas of bright ice when viewed in the animation.

The seven identified peaks are measured above a background value, which appears to include PIZ ice along the southeast coast of Ellesmere Island. We then subtract the background coverage of 5.6 km^2 from each peak. Summing these values results in a total ice flux of 75,300 km^2 with an associated uncertainty of 17% due to 0.25 dB in calibration accuracy. However, the mean backscatter of the ice exiting into Baffin Bay is 2.7-dB lower in backscatter than the PIZ ice measured in the Lincoln Sea. This decrease is due to mixing of PIZ ice with FY ice formed in the Strait. We use the mixture model described above to estimate the MY fraction of the ice exiting the Strait. The seasonal ice found in upper Baffin Bay has a mean backscatter of −15.2 dB with a standard deviation of 0.67 dB, while the perennial ice in the Lincoln Sea has a mean backscatter of −7.3 dB with a standard deviation of 0.24 dB. A perennial ice fraction of 0.45 results if these values are used. Accounting for these factors we estimate the export of the PIZ area through the Nares Strait to be ~34,000 km^2 with an uncertainty of 26%.

5.2. Deformation of PIZ

Divergence and convergence of the PIZ ice cover would add to or subtract from the total area of the PIZ. We use SSM/I ice motion fields to obtain an estimate of the net divergence/convergence of the interior of the PIZ. A polygon is used to define an initial area interior to the edge of the PIZ such that this area stays within our Arctic Ocean domain through May 1, 1997. The deformation of the PIZ area within our domain is what is of interest. We do not extend the polygon beyond the edge of the PIZ because of the lack of reliable motion data in some of these regions. On October 1, 1996, the vertices of this polygon are located on the nodes of a uniformly spaced ice motion grid (100 km by 100 km). The initial polygon vertices are selected on the basis of the location of these vertices on May 1, 1997. We require that these vertices remain within our domain over the 7-month period. The trajectories of the points are estimated using 1-day ice motion fields derived from sequential SSM/I data. Figure 12 shows the polygon at the beginning and end of the 7-month period. The final shape of the polygon seems to give a fair characterization of the motion and deformation of the PIZ interior compared to the boundaries of the PIZ.

Figure 13 shows the area of the polygon and PIZ area over the period. The initial area of the polygon is ~3.25 × 10^6 km^2. At the end of the 7 months, there is a net increase in area of 48,000 km^2, or 1.4% of the initial area. After detrending, the polygon area exhibits a variability of 25,000 km^2, or only 0.8% of the total area. This variability is much smaller compared to

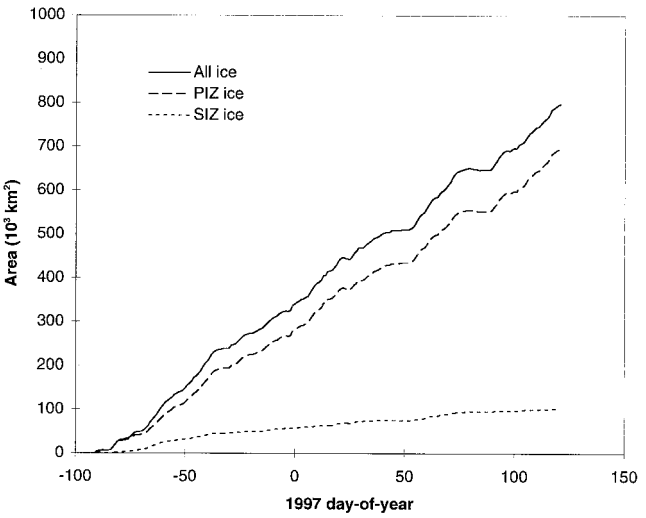

Figure 8. Total ice, PIZ ice, and SIZ ice area fluxes through the Fram Strait estimated using ice motion and NSCAT backscatter fields.

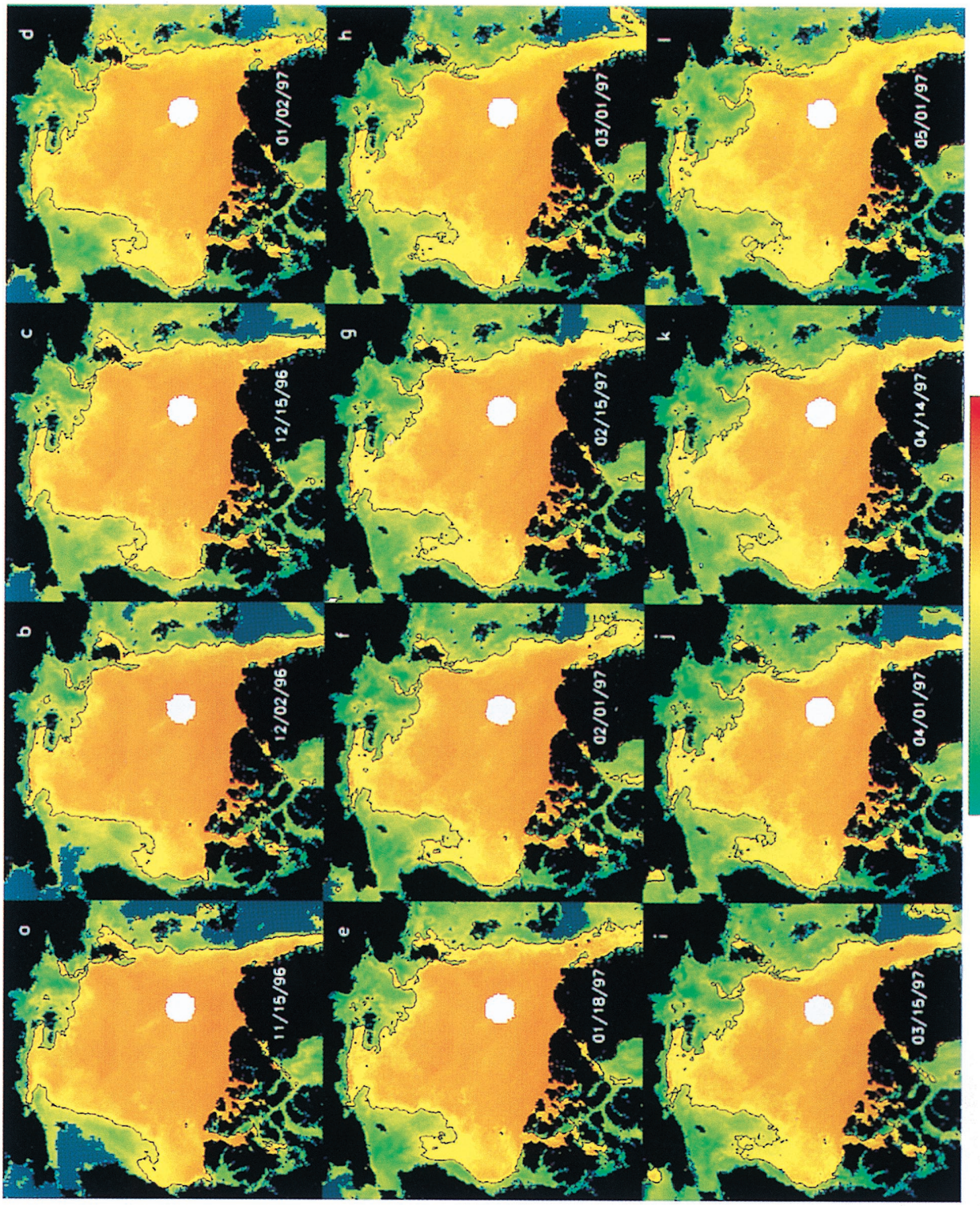

Plate 1. Sample of National Aeronautics and Space Administration scatterometer (NSCAT) backscatter fields from October 1, 1996, through May 1, 1997. The boundaries of the perennial ice zone are show in black.

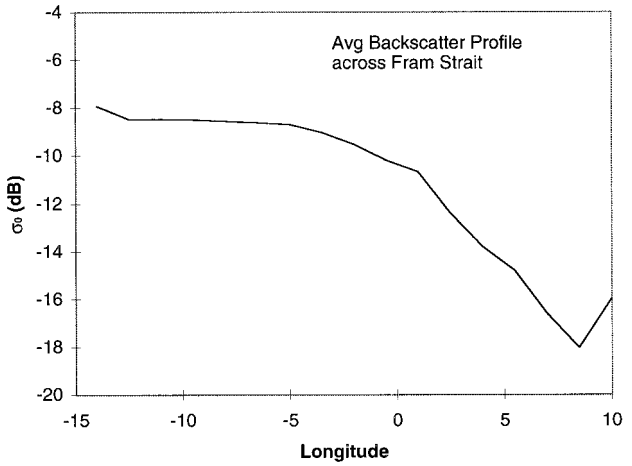

Figure 9. Profile of average backscatter of sea ice across Fram Strait over the 7-month period. The profile is sampled along a line approximately parallel to 81°N.

the variability of 62,000 km^2 in the PIZ area. Correlation of the detrended PIZ area and the area of the polygon gives $R = 0.55$. The deformation estimated with ice motion explains only a fraction of the variability of the derived PIZ area. Since the ice area within the interior of the PIZ appears to be changing little as a whole, the PIZ area exterior to the polygon must explain most of this variability. Indeed, the correlation of the detrended PIZ area outside the polygon and the PIZ area gives $R = 0.94$. The changes in the PIZ area outside the polygon explain more than 88% of the variance of the PIZ area, indicating that most of the variability occurs in the periphery of the PIZ. The question that we are not able to answer with this data set is Are MY ice areas at the end of the summer of 1997 added to the periphery of the surviving PIZ?

The above exercise gives us an estimate of only the net area change and the variability of the PIZ within the polygon. We do not, however, have an estimate of the $A_{\mathrm{def}}(t)$ term for the entire PIZ ice cover. If we assume that 1.4% is an indication of net divergence of the ice cover, then the net area increase of

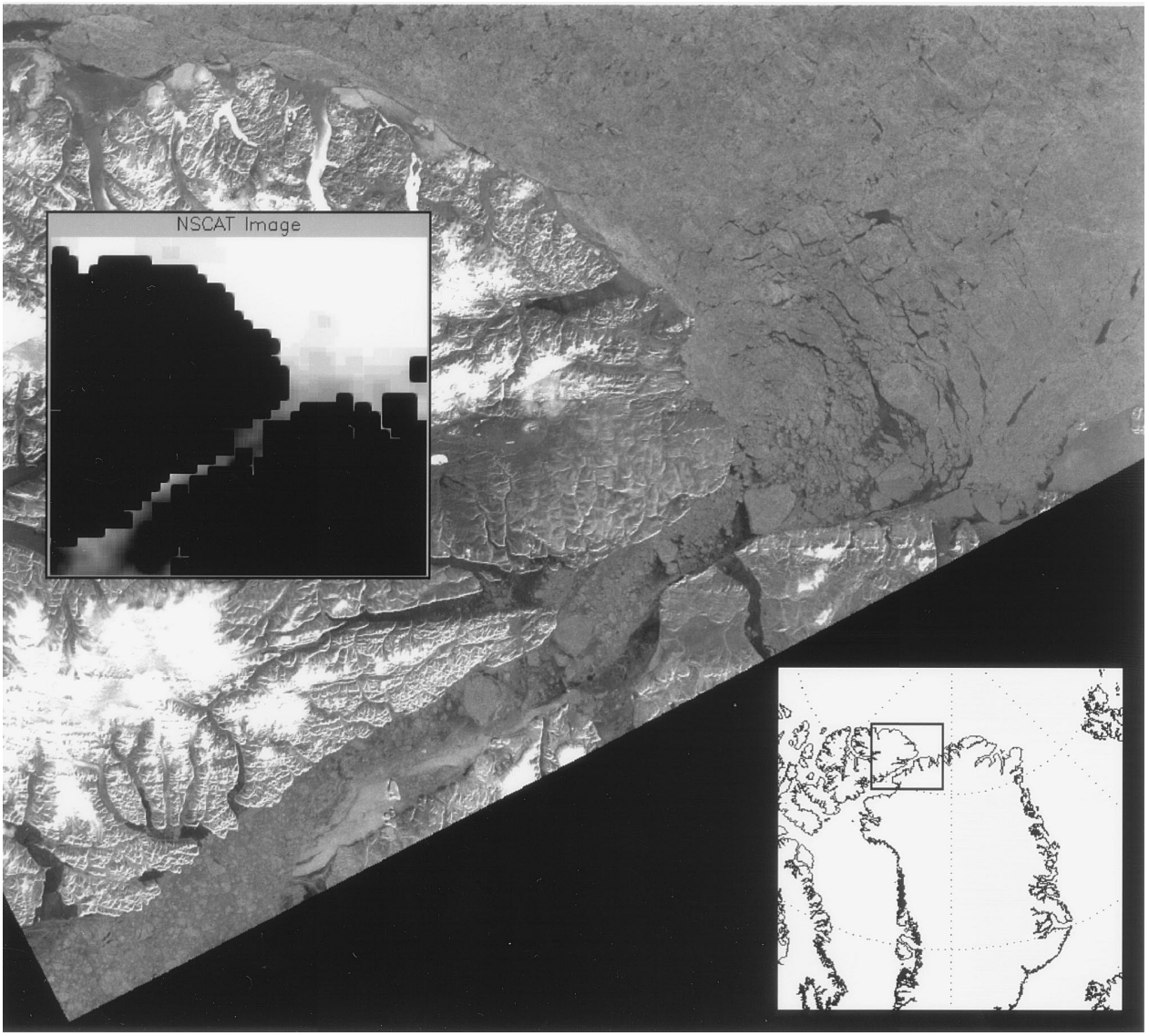

Figure 10. Coincident NSCAT and RADARSAT images of the Nares Strait on November 16, 1996. The insets show the low-resolution NSCAT backscatter of sea ice and the location of Nares Strait in north Greenland. (RADARSAT imagery ©CSA 1999)

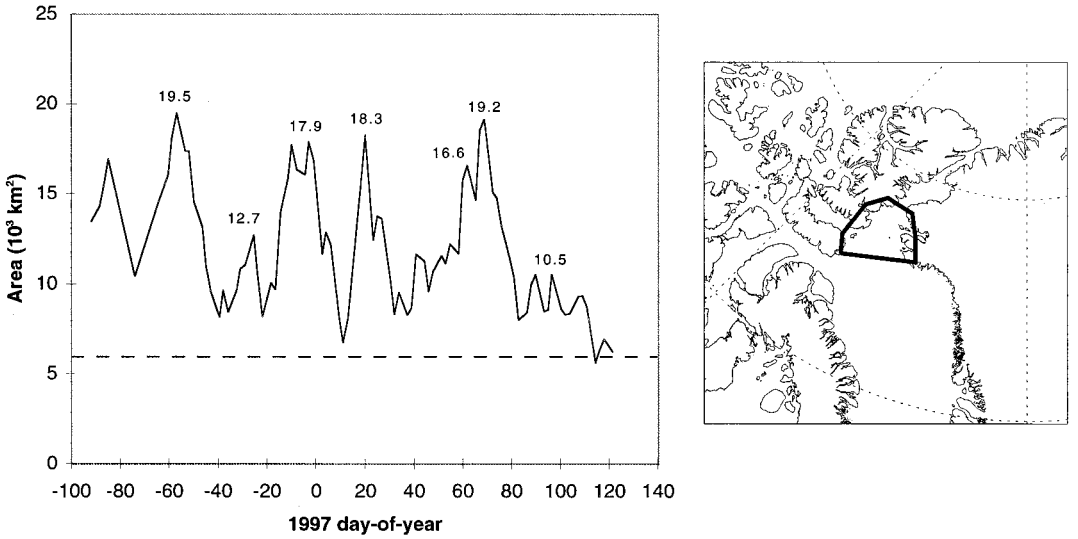

Figure 11. The PIZ ice area computed within a region south of the Nares Strait. (right) The area is computed using the backscatter information within the window. (left) The dashed line indicates background area removed from area flux calculations.

the ice cover over the 7-month period would be 78,500 km^2. This quantity, however, may not be indicative of the net divergence of the ice cover. We note that compared to the natural variability of the PIZ area of 1.3%, the 1.4% trend in the divergence computed here may not be significant. For example, the convergence of the ice cover at the north coast of Greenland and the Canadian Archipelago could easily reduce the total area change to zero. So, for the area balance computation here we left A_{def} as an unknown.

5.3. Discussion of Area Balance

Table 1 shows the area balance at the beginning of May 1997. Using the available estimates for terms in the PIZ area balance and their associated uncertainty, we are left with a residual of ~46,000 km^2 with an uncertainty of 111,000 km^2 on May 1, 1997. The uncertainty in this estimate is much larger than the mean and is dominated by the errors in the calculation of the PIZ area because of two factors mentioned above: (1) the determination of the thresholds and (2) the calibration accuracy of the sensor. The decrease in area of the PIZ over the period can be explained almost entirely by ice export through Fram Strait.

In the area balance we neglected the outflow of PIZ ice into the Canadian Archipelago, and the net deformation of the PIZ is left as an unknown. The outflow of PIZ ice through flux gates into the Canadian Archipelago is likely to be smaller than the uncertainty in our final estimates. If there is net divergence or convergence of the PIZ area, it would increase the unaccounted for PIZ ice area. Net divergence would give a positive residual and indicate that export of the PIZ area is underestimated, whereas net convergence indicates the contrary. A net divergence or convergence of 1% contributes ~50,000 km^2 to the imbalance. If indeed the net convergence/divergence of the PIZ ice cover is of the order of only 1–2%, then the unaccounted for area would change by the same amount.

5.4. Comparison With Passive Microwave Retrievals

Finally, we compare our PIZ area with the MY coverage of the Arctic Ocean derived from the SSM/I data. Figure 14 shows the ice area within our Arctic Ocean domain covered by more than 80, 60, and 30% concentrations of MY ice. Several features are evident: (1) our PIZ area estimates correspond to approximately the 30% coverage curve; (2) the variability of the two time series are correlated with the SSM/I-derived data having the higher of the two; and (3) both time series exhibit a downtrend over the 7-month period.

On the basis of our comparison with high-resolution RADARSAT imagery and assuming an average MY ice concentration of 90% within the PIZ we estimate that 68% of the Arctic Ocean is covered by MY ice on October 1, 1996. The passive microwave-derived data set gives a MY coverage of ~49%, significantly lower than our estimates. The underestimation of MY ice coverage by this data set and the possible causes have been noted by a number of investigators [*Comiso*, 1986; *Grenfell*, 1992; *Thomas*, 1993; *Beaven et al*., 1996; *Kwok et al*., 1996].

Perhaps the minimum ice area during the summer of 1996 would be a better comparison with our estimate. From SSM/I data the NASA Team algorithm estimates a minimum summer ice coverage of 61% (4.3×10^6 km^2) while the Bootstrap Algorithm gives a summer minimum of 67% (4.7×10^6 km^2). Our estimates could also be compared with the results of a filtering scheme described by *Thomas and Rothrock* [1993] and *Thomas et al*. [1996]. In their work a Kalman filter/smoother blends the results from a physical model with a SSM/I-derived ice type and concentration to obtain more consistent estimates of total ice and multiyear ice fractions. Their results show that over the period between 1979 and 1985, on the average, 60% of the area of Arctic Ocean is covered by MY ice. These results compare well with the 68% coverage we estimate for the beginning of October.

Other than the bias in the MY retrievals in the NSIDC data set, the correlation between the variability and the downtrend is interesting. The temporal variability may not be related to changes in the true concentration. We expect the shorter wavelength passive microwave measurements to be more sensitive to changes in the atmosphere and ice cover, thus giving the

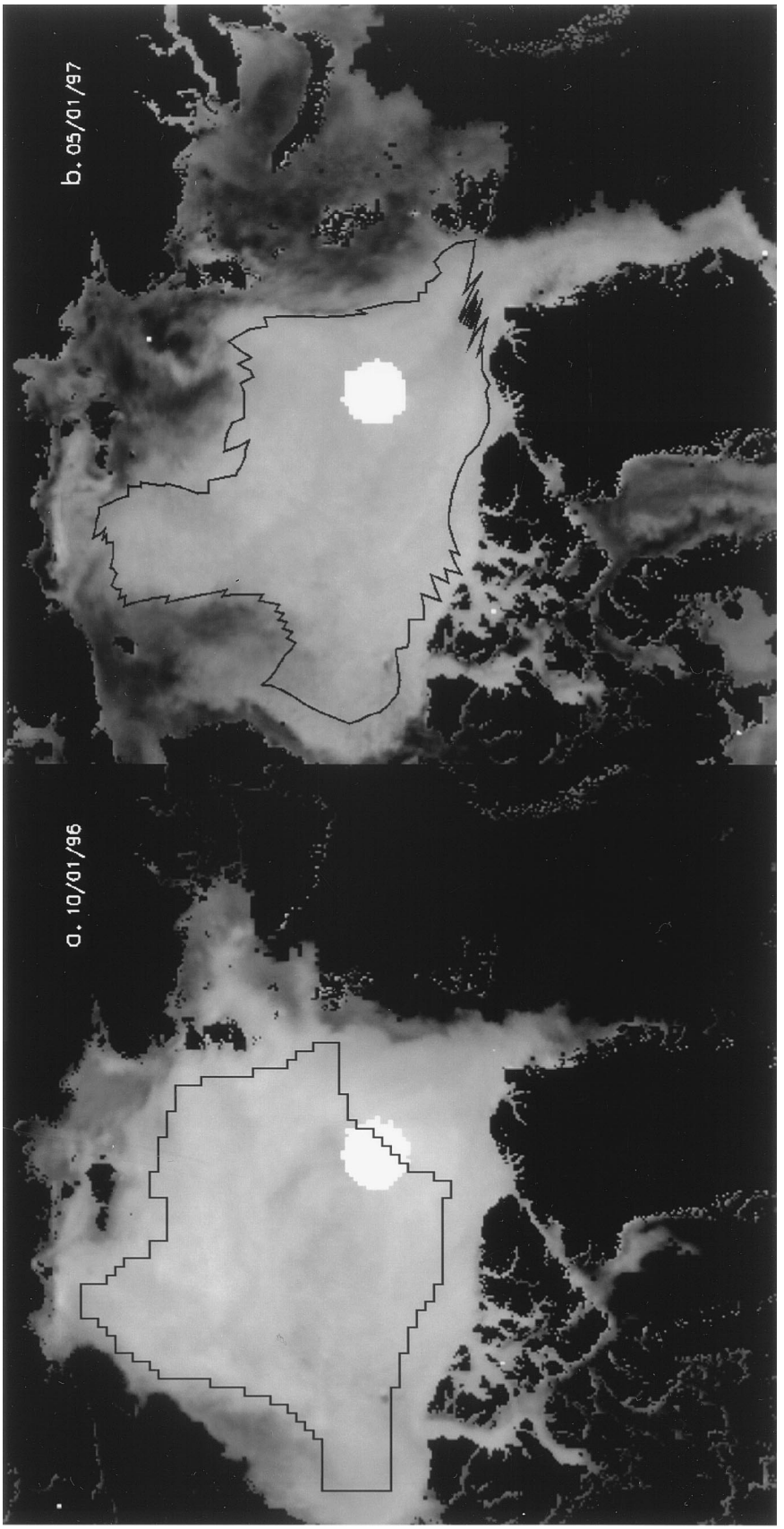

Figure 12. Deformation of the polygon defined within the PIZ boundaries: (a) October 1, 1996 and (b) May 1, 1997.

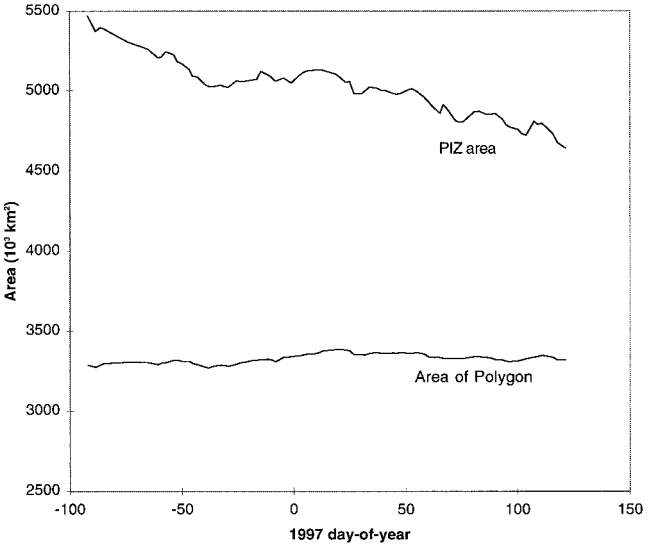

Figure 13. Comparison of changes in the polygon area inside the PIZ and the PIZ area.

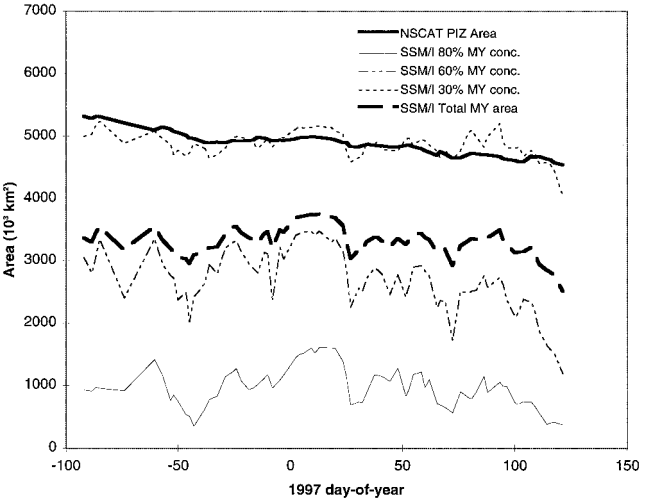

Figure 14. Comparison of the PIZ area with Arctic Ocean MY ice area coverage and ice area covered by more than 80%, 60% and 30% concentration of multiyear (MY) ice; MY concentrations are derived from satellite passive microwave brightness temperature.

time series a higher variability. The net change in the PIZ area, which can be explained almost entirely by ice export through the Fram Strait, can also be seen in the passive microwave data, although this trend is masked by the noisier MY area time-series from the passive microwave data.

6. Conclusions

The present contribution offers a new way to estimate the coverage of the PIZ using scatterometer data. We have shown through area balance that our interpretation of the backscatter fields from the NSCAT K_u band scatterometer is sound. RADARSAT and ice motion data have been used to understand the trend and the variability of the behavior of the PIZ area over the 7-month period. The quality and coverage of the NSCAT data and the stability of the backscatter of the ice cover are valuable for studying the ice cover.

The interesting results are as follows.

1. The PIZ area at the beginning of October 1996 occupies 5.32×10^6 km^2, ~76% of the Arctic Ocean. MY ice covers 68% of the Arctic Ocean, assuming a 90% MY ice concentration within the PIZ. The MY ice coverage compares favorably with the minimum ice area during the summer of 1996 estimated using passive microwave data.

2. By May 1, only 4.54×10^6 km^2 (covering 65% of the Arctic Ocean) of that area remains, a decrease of 0.78×10^6 km^2 over the 7-month period.

3. This area loss can be explained almost entirely by ice area flux through Fram Strait. Over this period the total area flux of sea ice through Fram Strait is 0.80×10^6 km^2, approximately 12% of the Arctic Ocean. Approximately 0.70×10^6 km^2 or 88% of that area is exported from the PIZ.

4. We estimate the PIZ area exported through Nares Strait to be 34,000 km^2.

5. After accounting for the outflow through the Fram and Nares Straits an unexplained residual of 46,000 km^2 remains. We attribute this residual to errors in our estimation process, the unaccounted for ice flux through the Canadian Archipelago, and the net divergence and convergence of the PIZ over the period.

6. The PIZ derived from K_u band scatterometer data provides an estimate of the MY ice coverage and its spatial distribution in the Arctic Ocean; the decrease in its area over the winter is an indicator of the ice area flux through the Fram Strait. Future K_u band scatterometers (e.g., QuikSCAT) have the potential of providing another complementary data set for monitoring the Arctic Sea ice cover.

Table 1. Area Balance of Perennial Ice Zone October 1, 1996, through May 1, 1997

Terms in (3)	Area ($\times 10^3$ km^2)	Uncertainty ($\times 10^3$ km^2)[a]
PIZ Area		
Area Change $[A_{PIZ}(0) - A_{PIZ}(t)]$	777	106
PIZ Ice Export (Net), A_{export}		
Fram Strait	697	31
Nares Strait	34	9
Canadian Archipelago	unknown[b]	unknown[b]
PIZ Ice Deformation (Net), A_{def}		
Area Change	unknown[b]	unknown[b]
Balance = $[A_{PIZ}(0) - A_{PIZ}(t)] - A_{export} - A_{def}$	46	111

[a]Total uncertainty is the root-sum-square of the column.
[b]These are unknown quantities, and they are discussed in the text.

Acknowledgments. The SSM/I data brightness temperature fields are provided by World Data Center-A for Glaciology/National Snow and Ice Data Center, University of Colorado, Boulder, CO. The RADARSAT data are provided by the Alaska SAR Facility, Fairbanks. R. Kwok, G. F. Cunningham, and S. Yueh performed this work at the Jet Propulsion Laboratory, California Institute of Technology under contract with the National Aeronautics and Space Administration.

References

Aagaard, K., and E. Carmack, The role of sea ice and other fresh water in the Arctic circulation, *J. Geophys. Res.*, *94*, 14,485–14,498, 1989.
Beaven, S. G., S. Gogineni, and F. D. Carsey, Fusion of satellite active

and passive microwave data for sea ice type concentration estimates, *IEEE Trans. Geosci. Remote Sens*., *34*, 1172–1183, 1996.
Carsey, F. D., Arctic sea ice distribution at end of summer from satellite microwave data, *J. Geophys. Res*., *87*, 5809–5835, 1982.
Cavalieri, D. J., P. Gloersen, and W. J. Campbell, Determination of sea ice parameters from Nimbus 7 SMMR, *J. Geophys. Res*., *89*, 5355–5369, 1984.
Comiso, J. C., Characteristics of winter sea ice from multi-spectral microwave observations, *J. Geophys. Res*., *91*, 975–994, 1986.
Comiso, J. C., Arctic multiyear ice classification and summer ice cover using passive microwave satellite data, *J. Geophys. Res*., *95*, 13,411–13,422, 1990.
Grenfell, T. C., Surface-based passive microwave studies of multiyear ice, *J. Geophys. Res*., *97*, 3485–3501, 1992.
Kwok, R., and G. F. Cunningham, Backscatter characteristics of the winter sea ice over in the Beaufort Sea, *J. Geophys. Res*., *99*, 7787–7803, 1994.
Kwok, R., and D. A. Rothrock, Variability of Fram Strait ice flux and North Atlantic oscillation, *J. Geophys. Res*., *104*, 5177–5189, 1999.
Kwok, R., E. Rignot, B. Holt, and R. G. Onstott, Identification of sea ice type in spaceborne SAR data, *J. Geophys. Res*., *97*, 2391–2402, 1992.
Kwok, R., J. C. Comiso, and G. F. Cunningham, Seasonal characteristics of the perennial sea ice cover of the Beaufort sea, *J. Geophys. Res*., *101*, 28,417–28,439, 1996.
Kwok, R., A. Schweiger, D. A. Rothrock, S. Pang, and C. Kottmeier, Sea ice motion from satellite passive microwave data assessed with ERS SAR and buoy data, *J. Geophys. Res*., *103*, 8191–8214, 1998.
Liebe, H., An update model for millimeter wave propagation in moist air, *Radio Sci*., *20*, 1069–1089, 1985.
Long, D. G., and M. Drinkwater, Cryosphere applications of NSCAT data, *IEEE Trans. Geosci. Remote Sens*., *37*, 1671–1684, 1999.
Naderi, F. M., M. H. Feilich, and D. G. Long, Spaceborne radar measurements of wind velocity over the ocean: An overview of the NSCAT scatterometer system, *Proc. IEEE*, *79*, 850–866, 1991.
Remund, Q. P., D. G. Long, and M. R. Drinkwater, Polar sea ice classification using enhanced resolution NSCAT data, paper presented at International Geoscience and Remote Sensing Symposium, Inst. of Electr. and Electr. Eng., Seattle, Washington, 1998.
Thomas, D. R., Arctic sea ice signatures for passive microwave algorithms, *J. Geophys. Res*., *98*, 10,037–10,052, 1993.
Thomas, D. R., and D. A. Rothrock, The Arctic Ocean ice balance: A Kalman filter smoother estimate, *J. Geophys. Res*., *98*, 10,053–10,067, 1993.
Thomas, D., S. Martin, D. Rothrock, and M. Steele, Assimilating satellite concentration data into an Arctic sea ice mass balance model, 1979–1985, *J. Geophys. Res*., *101*, 20,849–20,868, 1996.
Ulaby, F., R. K. Moore, and A. K. Fung, *Microwave Remote Sensing: Active and Passive*, vol. I, *Microwave Remote Sensing Fundamentals and Radiometry*, Addison-Wesley, Reading, Mass., 1981.
Wittmann, W. I., and J. Schule Jr., Comments on the mass budget of Arctic ice pack, in *Proceedings of the Symposium on the Arctic Heat Budget and Atmospheric Circulation*, edited by J. O. Fletcher, pp. 215–246, Rand, Santa Monica, Calif., 1966.
Yueh, S., and R. Kwok, Arctic sea ice extent and melt-onset from NSCAT observations, *Geophys. Res. Lett*., *25*, 4369–4372, 1998.
Yueh, S., R. Kwok, S. H. Lou, and W. Y. Tsai, Sea ice identification using dual-polarized Ku-band scatterometer data, *IEEE Trans. Geosci. Remote Sens*., *35*, 560–569, 1997.

G. F. Cunningham, R. Kwok, and S. Yueh, Jet Propulsion Laboratory, California Institute of Technology, 4800 Oak Grove Drive, Pasadena, CA 91109. (ron@rgps1.jpl.nasa.gov)

(Received December 7, 1998; revised July 9, 1999;
accepted August 4, 1999.)